Tribology International 188 (2023) 108858

Contents lists available at ScienceDirect

Tribology International

journal homepage: www.elsevier.com/locate/triboint

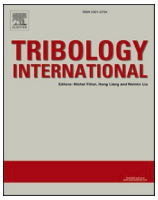

Experimental investigation of the effects of load path on the life of fretting fatigue contacts

Luke Blades *, James Truelove, Robert Paynter, David Hills

Department of Engineering Science, University of Oxford, Parks Road, Oxford OX1 3PJ, UK

ARTICLE INFO

Keywords:
Fretting
Fatigue
Wear
Crack measurement

ABSTRACT

Slip and changes to stresses within a load cycle both contribute to damage in fretting contacts. By considering conditions for slip in normal-bulk loaded fretting contacts, experiments were performed wherein the contact slip varied, whilst changes to stress were modest. This was achieved by keeping the load endpoints constant but altering the load path. Experiments showed stark contrast in life between tests permitting slip and those prohibiting it. FE models were used to plot slip and stress components, revealing that the differences in life were due to a combination of slip and changes in shear traction. A method is presented by which the crack position can be measured, by adding a feature to the pad to produce a datum mark.

1. Introduction

Fretting fatigue is a damage mechanism which is common in highly loaded, nominally static contacts subject to vibration or otherwise cyclic loading (a number of examples are given in [1]). The initiation of cracks at the edges of these contacts is often attributed to high stresses and stress gradients, and many methods of life prediction have been developed to predict this initiation life [2]. It is very common for these assessments to be made based on combinations of stresses and tractions at the contact edge [3], whilst slip is only considered insofar as it modifies the stresses and tractions. Slip is usually considered more important in fretting wear problems and often disregarded in fretting fatigue [4]. Attempts have been made to quantify the effects of slip on the life of fretting contacts. However changes to slip between tests have been produced by changes to loading, which also substantially changes the stress variation [5,6]. Decoupling these effects is key to understanding the separate effects of the state of stress and slip on initiation life.

It is not simple to achieve this, since they're both driven by the same load and geometry parameters. Any slip will necessarily relieve the state of stress, making true decoupling impossible. The method presented here was to alter the path taken through the load-space, whilst keeping the end-points of the load path common between tests. The advantage to this method is that very large changes can be made to the slip zone, with relatively modest changes to the state of stress. It was found that sequentially loaded specimens (a load path which promoted slip) failed after few cycles, whilst proportionally loaded contacts (following a load path prohibiting slip) reached the run-out cycle count of two million. Further testing was then performed using intermediate load paths, to find how the life varied between the two extremes. Whilst these tests do not fully decouple slip from shear traction, it is shown that the coupling of slip with the bulk tension at the surface is almost eliminated by this test method.

Finally the novel concept of adding a small 'denting' feature to the pad face to provide a datum for crack position measurement was tested. The crack positions and lives of these tests showed good repeatability. The positions of cracks were compared with the output of FE models allowing assessment of the various stress components and dissipated energy values at the site of initiation as possible nucleation drivers.

2. Background and theory

This paper reports on a number of fretting fatigue experiments performed by pressing pads into the sides of dogbone specimens, and loaded as shown in Fig. 1. The behaviour of the contact is controlled by the four loads shown, the normal pad force 'P', the shear force 'Q', the differential bulk tension 'σ_B' and a pad moment 'M'. Most practical fretting fatigue experiments are uncoupled, meaning that the normal contact problem depends only upon the pad and moment loads, whereas the shear problem is excited by the bulk tension and shear load. When modelling fretting fatigue experiments analytically it is common to represent the contact using half plane theory; in this model the two contacting bodies are represented as infinitely large half planes. If the

* Correspondence to: University of Oxford, UK.
E-mail address: luke.blades@eng.ox.ac.uk (L. Blades).

https://doi.org/10.1016/j.triboint.2023.108858
Received 20 December 2022; Received in revised form 25 July 2023; Accepted 3 August 2023
Available online 6 August 2023

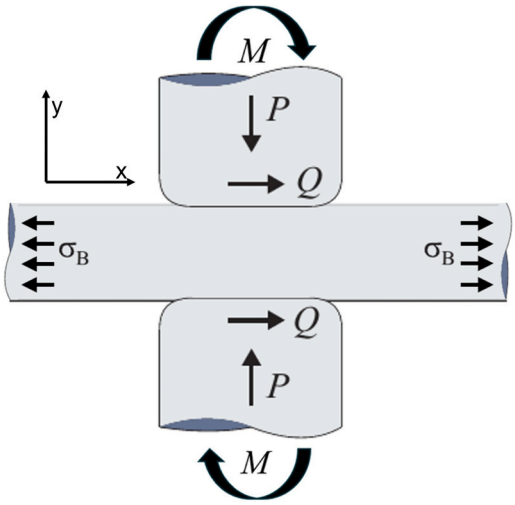

Fig. 1. Diagram of the specimens and pads with the required components of loading; the normal load 'P', the shear load 'Q', the moment across the pad 'M' and the bulk tension 'σ_B'.

contacting components are elastically similar the problem is said to be uncoupled: in particular the tangential solution does not affect the normal solution or vice versa.

The study of bulk tension loaded contacts following arbitrary load paths was considered by Ramesh et al. [7], who considered the specific case of a contact following an elliptical loop in 'P', 'σ' load space. The solutions used here are built up via superposition of partial slip and fully stuck shear traction solutions, following the same methods described in the work by Ramesh but applied to different loading histories.

When a contact undergoes an increment of loading the condition for no slip is given by [8],

$$\frac{\Delta Q}{\Delta P} + \frac{\pi a \Delta \sigma}{4 \Delta P} < f \tag{1}$$

where 'a' is the half-width of the contact and 'f' is the coefficient of friction. Notice that for a 'P-Q' problem, this full-stick condition reduces to a fixed maximum gradient equal to the coefficient of friction, so that the contact will remain stuck everywhere through an increment in loading that is below this gradient. For a 'P-σ' problem, however, equation 1 is a function of the contact width, so that as the normal load increases and the contact grows the maximum permitted increment of 'σ' to maintain full stick decreases.

In our complementary paper [9] we apply the principles derived by Ramesh et al. to a selection of load paths having properties relevant to fretting fatigue experiments. These include proportional and sequential tests used to probe the effect of the existence of slip, the 'hockey stick' (intermediate path) load paths used to investigate the effect of the size of the slip zone and the slip displacements, and triangular loops used to investigate the effect of slip direction.

2.1. Half-plane idealisation in analytical theory

Finite element models *and* closed form elastic half-plane analysis are both used in this paper to interpret the results of the experiments performed. Closed form analysis allows the use of exact solutions to approximations of the experimental condition, which in this case, required the representation of the elastic domain in each of the contacting bodies as half-planes. This assumption neglects two key aspects of the problem. First that the contact defining body has a finite form (the pads extend only a millimetre beyond the contact) and so the surrounding material is removed relative to the half plane assumption, lowering the stiffness. This pad domain shape is the most obvious difference, but secondly the most significant error of the half-plane approximation, in this case, is the representation of the dogbone as having infinite thickness. As shown in Fig. 1, the contact is 'mirrored' (a pad on each side) across the dogbone which is 10 mm thick in the experiments modelled, so in effect, there is a line of symmetry 5 mm from the surface, rather than an infinite elastic half-space.

Fig. 2 shows a comparison of the tractions obtained by both methods of analysis. This shows the maximum (absolute) values of the shear traction over the course of one sequential loading cycle. The pressure shown is at maximum normal load, indicating also the maximum contact size predicted by the two methods. Note that the stiffer contact resulting from the more realistic FE boundary condition gives a smaller (by more than 1 mm) contact size, and correspondingly larger tractions, indicating that for life prediction of these contacts, the FE modelling may be the more conservative option. Section 2.2 deals with measured crack positions compared with positions of peak values of stress and energy dissipation, also required output from the FE modelling, as the contact size and positions of these maxima were critical.

2.2. Crack position measurement

The second novel method assessed in this paper is the use of a small feature machined onto the contact defining body, used to locate the crack relative to the position of the contact defining body. Whilst the FE analysis allows us to find an approximation for the dissipated energy or any stress component at any point throughout a load cycle, correlating this to the position of the real crack is not simple. Images of the contact patches of completed tests (Fig. 3a and b) show clearly that objective identification of the 'edge' of contact is very difficult, as there are no clear registration points from which the crack can be measured.

Whilst the slip zones are visible, clearly and objectively defining their extremes is not possible to length scales of 0.1 mm, across which significant changes in tractions and cumulative energy dissipation can occur. Also, even with a high resolution image, clear and objective identification of the 1D 'position' of the crack (for comparison with output from 2D analyses), is not obvious, as the crack rarely runs straight across the specimen (again, clear in Fig. 3a). The variation in this crack initiation position has been attributed to the change in condition from plane strain near the centre of the dogbone, to plane stress at the dogbone free surface. It was noted from observation of the specimens post-test, that consistently both the slip zones and the crack distances (along the dogbone, from the centre of the contact) were larger at the edges of the dogbone than in the centre. Since the half-plane analysis is valid only under conditions of plane strain, the centre third of the contact was used for crack position measurement, where the size of the slip zone and the crack position appeared to be relatively consistent (in position within each test, whilst there is some variation in the crack position between tests). Note that we make this assumption because from inspection of the crack surfaces of the failure specimens, no edge

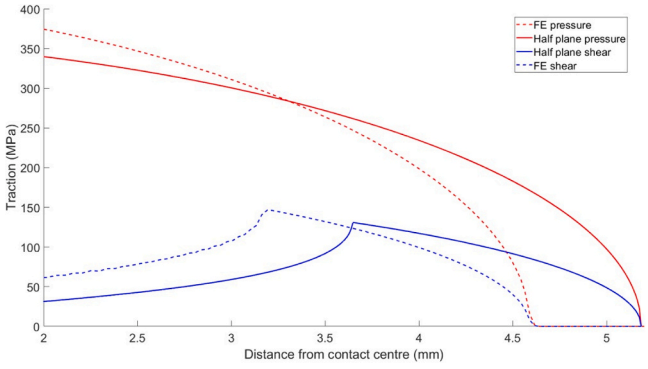

Fig. 2. Graph of the tractions of the experimental contacts as predicted by analytical solutions and by FE modelling. The conditions are from the 100 % sequential case as described in Section 3.1.

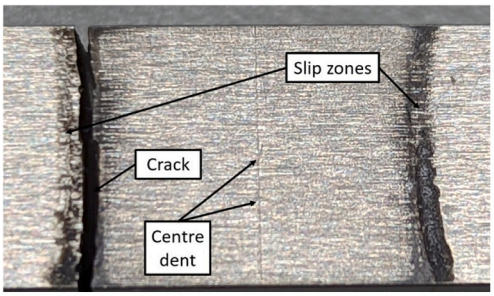

(a) The contact interface after the test; note the subtle indentation in the centre of the contact.

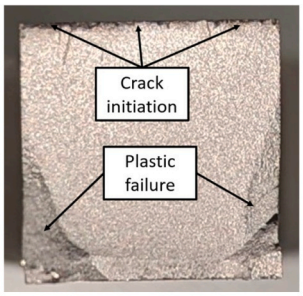

(b) The fracture surface, and the even distribution of initiation beaching marks at the top of the image.

Fig. 3. Photographs of failed specimens.

initiation was found (example given in Fig. 3b).

The geometry chosen for a trial was a pad having an 8 mm flat, but with a large 200 mm edge radius to give a large slip zone. A large slip zone was required so that the position of the crack within this slip zone could be clearly identified and correlated with output from the analysis, as the gradients of the stresses are lower. The added feature (described fully in Section 3.1) was applied using a wire EDM, which was the typical manufacturing method for pads in this test programme. Use of this denting feature is only possible for pads with a flat (either fully complete contacts or those with flat/round faces). Hertzian pads cannot be used, as any minor rolling of the pad would move the dent away from the centre. This minor rolling is not possible in flat and rounded contacts as the flat portion provides a small but necessary correcting moment. When comparing contacts with this denting feature and without, clearly the stresses will be quite different at the centre of the contact. However though careful design, it was shown (by FE) that the difference in stress state and slip at the contact edge was negligible.

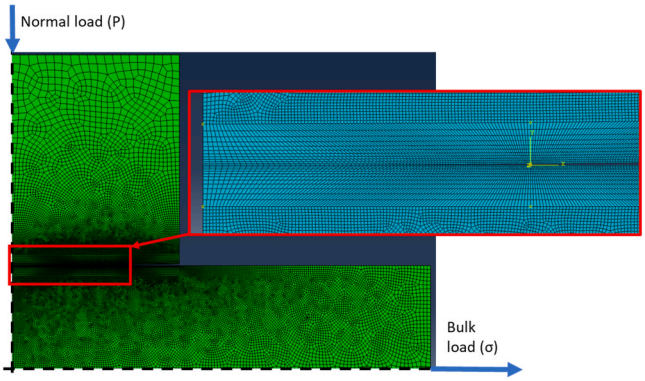

Fig. 4. FE model structure, mesh, boundary conditions and loading. The model takes advantage of symmetry conditions along the left and lower edges. The normal and bulk loads are applied at points along these lines of symmetry.

2.3. FE modelling

The Finite Element simulation was carried out using the Abaqus implicit analysis package. This can model non-linear phenomena including contacts and material effects such as plasticity, though the models used in this paper were fully elastic as stresses were not high enough to cause any plasticity. Each non-linear feature adds difficulty in obtaining a solution. In most cases the solution cannot then be found in a single step, so iteration is used, solving each part in order then convergence is checked, if not satisfied the load increment is reduced until convergence is satisfactory. In the case of frictional contact the normal component is found, then the tangential. The normal contact was set to the Abaqus 'hard' condition, in which over-closure is minimised, and the tangential behaviour was defined by the standard 'Lagrange multiplier' method. If the increments are allowed to be large then the resulting solution can have a 'jagged' nature in the shear traction distributions found; overly large element size affects results similarly. Typical incrementation for clean results required 40 steps. As the problem is symmetrical both in loading and geometrically, this was exploited to reduce the model to a quarter of the geometry; the boundary conditions on the lower and left hand edges of the model are symmetry in their respective lines. The model uses plane strain elements (Abaqus designation CPE4R). The mesh is fine at the contact interface and element size is biased smallest near the edge of contact (20 μm). Coarser meshing (400 μm) was used away from the contact where stress gradients were lesser to lower simulation times (Fig. 4).

3. Experimental setup

The tests were performed on a piece of bespoke test apparatus built at the University of Oxford, shown in Fig. 5a. The tangs of a dogbone specimen (shown in Fig. 5b) are held in clamps, each connected to a hydraulic actuator with 200 kN capacity. The top and bottom actuators allow for independent control of the shear and bulk tension ('Q' and 'σ'), though only the bulk tension is varied here, so the actuators pulled with nominally equal force at all times. The two other load components required to define the fretting contact are the normal force and moment across the contact. The normal force is applied by a third horizontal actuator which rests in a floating caliper, so an equal force is applied to each of the two pads. The pad holding blocks are supported by shear reaction plate springs (shown in Fig. 5b) that lie in the plane of the contact of their respective pad, eliminating any shear- moment coupling. It is also worth noting that in the experiments performed here (except the crack position measurement tests), the pads were Hertzian in geometry and so could not support a moment. Consequently, the stresses in the contact studied are the result of only two external load components, which are the Normal load 'P' and the Bulk load 'σ'. For the test results presented, the maximum and minimum values of these load components were common. It is the route through the 'P-σ' load-space that is changed between tests of the same set in this test programme. Most practical fretting fatigue experiments are uncoupled, meaning that the normal contact problem depends only upon the pad and moment loads, whereas the shear problem is excited by the bulk tension and shear load. The rig was initially designed around the principles of asymptotic matching [10], which implies that the four load components can be reduced to a two parameter space; for this reason no moment control was included in the rig. This experiments were performed in a lab at 22 degrees and humidity was not measured.

Fig. 6 is a graph of this load space and shows important features for the specification of the chosen load paths. The parameters of this experiment were chosen with three criteria. First, the contact must not yield anywhere (besides surface asperity yield), as this would invalidate the elastic analysis. Second, the contact must not slip at the edge when

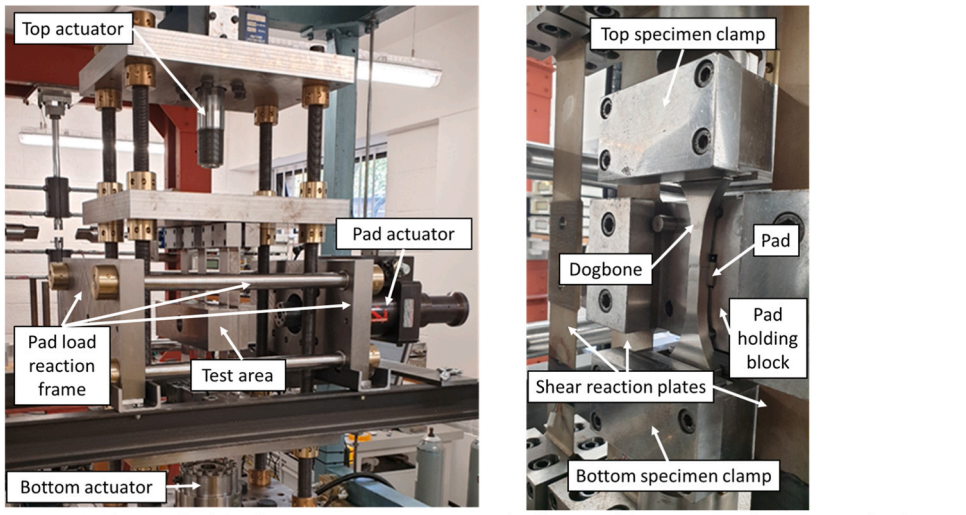

(a) Photograph of the Cornerstone rig (b) Close up of the test area with specimen and pad in-situ

Fig. 5. (a) Photograph of the Cornerstone rig. (b) Close up of the test area with specimen and pad in-situ.

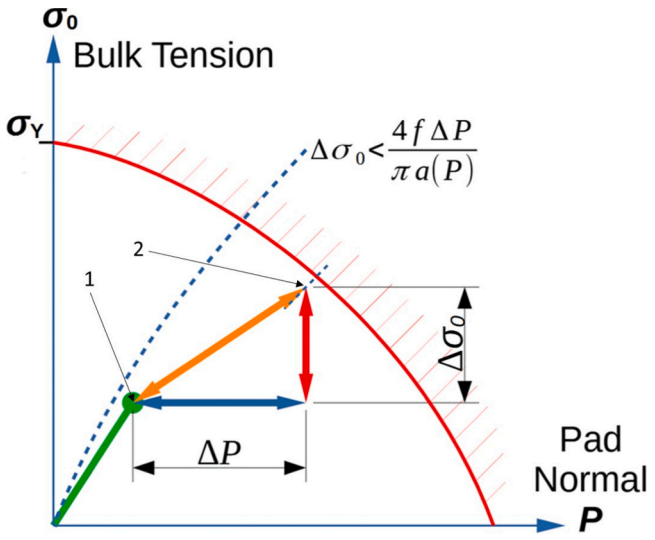

Fig. 6. A graph of the 'P-σ' load space and relevant features used to define the load paths taken in these experiments. The dotted blue line represents the no-slip inequality. The solid curved line represents the elastic limit, which must not be exceeded if the elastic half-plane analysis is to be useful. The solid green line beginning at the origin shows the initial loading step, and the other arrows illustrate the load paths taken.

proportionally loaded, this sets the critical maximum gradient and requires a knowledge of the coefficient of friction. This allows comparison between tests with slip and those which were nominally stuck throughout the entire load cycle. Third, the experiment must produce specimen lives which can be compared, i.e two run-outs would be useless. This requires a significant $\Delta\sigma$, so that any nucleated crack are able to propagate).

These criteria cannot be achieved for all materials and contact geometries as, for example, often the stress required to achieve criterion 3 is often too high to satisfy criterion 1. In planning a test, first, the lower load point (figure 6 point 1) was chosen, requiring a small positive pad load and dogbone tension to eliminate backlash related control problems associated with moving between tension and compression in load paths. The load state at the upper load point, 6 Point 2, was then chosen considering the position of point 1 and the criteria above. To satisfy criterion 1 (no yield), the experimental contact was analysed using a finite element (FE) model, and a safety factor was applied to allow for experimental misalignment or modelling error. Note that it is possible to find an analytical solution for the elastic limit curve in 'P'-'σ' space, but this requires the assumption that the dogbone behaves like a semi-infinite half-space, which is not valid here due to the 10 mm dogbone width and presence of the second opposing contact, which raises the state of stress. In fact, for Hertzian contacts with a radius that is large relative to the dogbone thickness (distance between the opposing pads), the highest von Mises stress occurs in the centre of the dogbone, with contributions from each of the two contacts. Criterion 2 was met by satisfying the incomplete contact full stick condition given in Eq. 1. This condition was confirmed by the FE analysis.

This means that in Fig. 6, the gradient of the line passing through points 1 and 2 (the proportional loading path), must be less than the gradient of Eq. 1, plotted with a dotted line, at the maximum P value of that test. The third condition was satisfied through use of a minimum bulk stress variation (required to propagate cracks to failure) and the variation in geometric parameters of the contact, which was the radius of the Hertzian pads. Note, this has some interdependence with criterion 1.

3.1. Test specification

In all the experiments described, the loading and unloading paths, in 'P-σ' space, are coincident, that is, there are no 'loops'. In qualitative terms, the steeper the gradient of the loading line in 'P-σ' space, the more likely there is to be slip, and, when there is slip, the larger the slip zones will be, particularly at larger loads when the contact size increases. Fig. 7a shows the range of paths taken. At one extreme, the left hand, green line - the one for proportional loading, is chosen so that, even at the largest contact size, there will be no slip present. In all other cases there is at least some normal load applied before the tension and normal loads are increased in proportion and, in the most extreme form of this, the red line at the right where the normal load is applied up to Point 2 (7a), and then the tension added, there will certainly be forwards slip during loading, and reversing slip during unloading. The intermediate lines define load paths whose properties lie between these extremes. We need a notation to describe their shape, and the one adopted is to denote the length of the normal-load-only part of the path as a fraction of the length (Point 2 - Point 1), as shown.

Two sets of tests are reported here. In the first set of 8 tests, each of load paths represented in Fig. 7a were followed. The lower load point (marked point 1) has coordinates P = 300 N/mm, σ = 40 MPa. Point 2

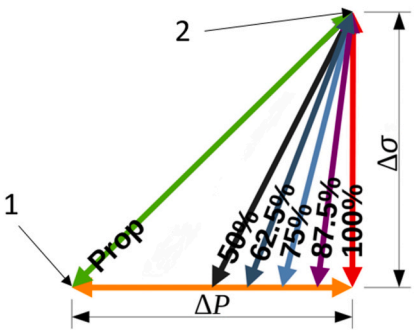

(a) A graphical description of the proportional, sequential (100%) and hybrid load paths performed in this test set on a flat and round geometry and in the following section on the Hertz geometry.

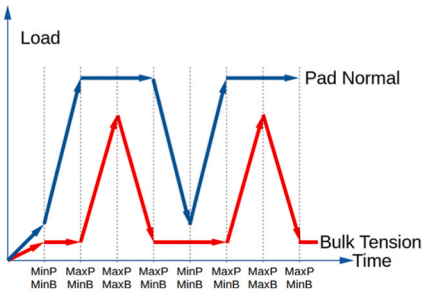

(b) A graph of the two load components against time for the fully sequential case.

Fig. 7. Descriptions of the load paths taken in the P-σ and time domains.

has coordinates P = 3000 N/mm, $\sigma = 280$ MPa. These loads were applied as shown in Fig. 1, and Fig. 7b shows the 100% sequential load path in the time domain for the two load components. These load points are common for all tests presented in this paper and the path taken between them in a load cycle was varied between tests. All tests in this set were performed with Ti-6Al-4V titanium alloy specimens and pads. The 0.2% yield strength of this material was measured at 900 MPa and the coefficient of friction was measured at 0.5. The contact geometry was Hertzian with a radius of 450 mm, and the tests were performed at a frequency of 4 Hz. The tests were run until the specimen failed completely (crack propagated all the way through) or until the cycle count reached the run-out value of 2,000,000. The roughness (measured in the direction of the applied shear load) was 2 μm Ra in the dogbone which was finished on a surface grinder, whilst the pads were finished with a wire EDM machine and measured at 0.6 μm Ra.

The second set of experiments was to exploit the novel method of crack position measurement. Six identical tests were performed to study the repeatability of crack formation position and the life of the contact. These tests were also performed with Ti-6Al-4 V specimens. The pads were made from the same material but with a different geometry from the previous set; the pad geometry used in these tests consisted of a flat central portion 8 mm wide, with a radius of 200 mm at each end. In the middle of the flat portion of the pad, a small feature described in Fig. 8 was added, designed to produce a dent on the dogbone. The same load points were used as in the first test set, and the 100% sequential path was followed for all tests of this set.

4. Experimental results

The results from the first set of tests are shown in Fig. 9. This graph

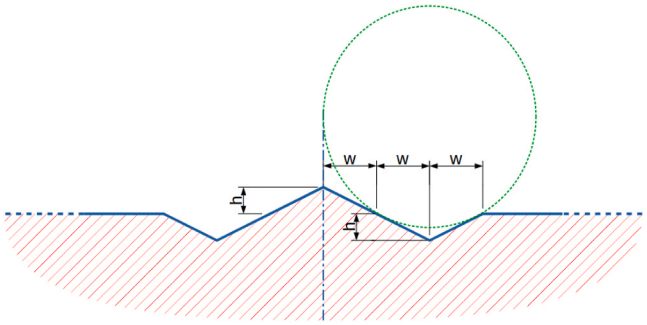

Fig. 8. A diagram of the geometry of the central denting feature EDM machined onto the pads in this test set. The value of 'h' was 5 μm and 'w' was 25 μm. The dotted green circle represents the EDM wire used to machine the pad, and indicates the true geometry of the dent feature roots.

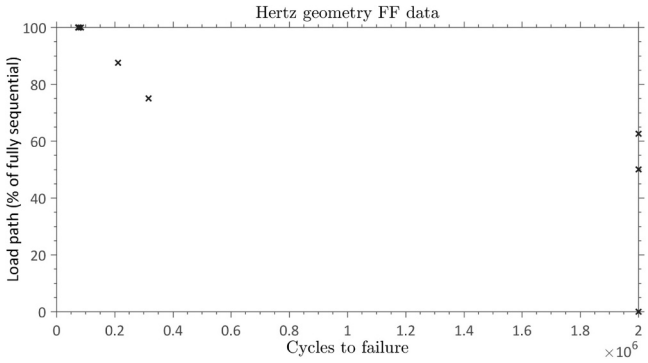

Fig. 9. Graphed data for the Hertzian sequential, proportional and hybrid tests.

shows the lives of the specimens against the load path to which they were subjected. Load paths 62.5 % and below went to run out (2,000,000 cycles), and no cracking was visible in any of these specimens. The remainder of the tests failed between 80,000 and 320,000 cycles, with the more sequential paths resulting in shorter lives. Three tests were performed with the 100% sequential path, and the lives of these were 75,000 77,000 and 83,000, indicating good repeatability of the apparatus.

As described in Section 3, the load path followed in the fully proportional test should result in a contact with no slip, whilst the proportional paths will have significant slip in the contact edge. The images in Fig. 10 confirm a significant difference in the degree of surface damage resulting from these two load cases. The left hand image in this figure shows the damage to the dogbone specimen after 2,000,000 cycles of proportional loading, which is minimal, confined to the centre of the contact, and likely due to the asperity damage at relatively higher pressures. The right hand image shows the significant oxidation of the surface in the slipping regions of the sequentially loaded contact, after

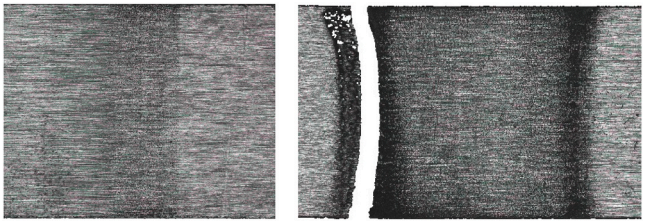

Fig. 10. Images of the proportionally loaded (left) and 100% sequentially loaded (right) dogbone contact regions, post-test. Note that the sequentially loaded contact shows significant surface damage, along with a fatigue crack.

only 75,000 cycles (time of failure). Clearly the change in load path resulted in significantly different slip behaviour in the experiments.

4.1. Crack position measurement results

Six tests were performed under nominally identical conditions and the specimen lives varied between 59,000 and 130,000 cycles. The failed specimens were then imaged using an 'Alicona' scanning microscope. Even with the 3D scan data achieved by focus variation, the precise location of the crack in the plane of the specimen surface was not reliably identifiable, so minimum and maximum distances between the centre dent and the crack (within the centre third of the dogbone as explained in Section 2.2) were taken for each specimen. These distances are plotted in Fig. 11b. The data indicate much more consistency in the outer crack position (maximum distance from contact centre) than in the minimum distance measurements. The outer crack positions have a range of just 30 μm across all 6 tests whilst the inner crack positions had a range of 147 μm, with no obvious outliers. There was no correlation between any of these crack position measurements and the number of cycles to failure of a specimen.

5. Discussion

5.1. Load path testing

The results from the load path variation testing indicate strongly that for the contact considered, the path taken though load space has a significant effect on life. At the crack initiation site, there are three stress components to consider, as well as the relative motion between the dogbone and specimen, which must be compared between the load cases. This information was found by FE modelling of the load paths. The first load component, pressure, did not change substantially between cases, and was not plotted. The shear traction for each load case is plotted in Fig. 12, the tension parallel with the contact (Sxx) is plotted in Fig. 13, and the dissipated energy is given in Fig. 14.

First we consider the effect of varying the load path on the shear traction in the contact. Note that in this analysis, negative tractions occur during loading, with the dogbone placed in tension, dragging the dogbone outwards beneath the pad. Here, unlike with the direct traction, we see some significant variation with load path. The plot in Fig. 12 shows the minimum and maximum values of shear traction over one cycle against distance from the centre of the contact, for the right hand edge of the contact. The first observation to make is that it is only the positive traction which changes from case to case, and that the minimum traction is independent of the load path taken. The similarity in minimum shear traction between these cases is because they are all above the condition for identical states of slip [9]. This means that the shear traction distribution is therefore also identical in all cases, consisting of just a partial slip term with contact size a and stick zone size a_k. Any differential surface strains locked into the contact under full stick portions of the loading cycle occur in regions which are subsequently within the slip zone, and as such are erased during the later portions of the load path. The positive shear tractions, in contrast, occur during the unloading stage of the contact, and do depend upon the path taken during unloading. The shear traction in the reverse slip zone is equal to the coefficient of friction multiplied by the contact pressure, so the magnitude of the shear traction depends upon the gradient at which the normal load is unloaded, if the contact is unloaded at a higher normal load the shear traction will be larger in magnitude.

Next we considering the range of the Sxx stress, plotted in Fig. 13. In all cases the peak value was approximately 4.6 mm from the contact centre, corresponding to 50 μm in from the edge of the contact at its maximum extent, with a value of 540 MPa. No significant difference in this stress range was found across all load paths studied for points in the contact further than 4.1 mm from the centre. Closer to the centre of the contact, some difference in this stress range is seen. These positions, however, are removed from the expected crack initiation site (which is close to the highest Sxx range as found in Section 5.2). This indicates that the difference in life between load paths is unlikely to be due to variation in Sxx range at the crack initiation site.

This contact geometry and the positions of the end points in load space were designed such that a proportional (0 %) path would result in no slip. The dissipated energy in the slipping cases is plotted in Fig. 14. The more sequential paths dissipate a larger amount of energy per cycle, both in a point-wise sense and consequently in total (the integral of the curves shown). The more sequential paths also result in energy dissipation distributions with a stronger skew towards the edge of contact. The results from the FE output indicate that the changes to contact life observed with changes to load path are not due to differences in Sxx stress or to pressure, but to changes in shear traction range, dissipated energy, or both. It is not possible to decouple the effects of shear traction range and dissipated energy with the load paths presented here.

5.2. Crack position measurement

The average extreme positions of the cracks from these 6 tests were

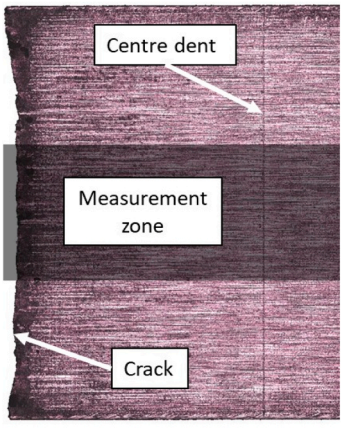

(a) An annotated profilometer micrograph of the contact surface of a failed dogbone with dent formed by the central pad feature. The crack is on the left hand side of the image and the dogbone extends out of frame to the right.

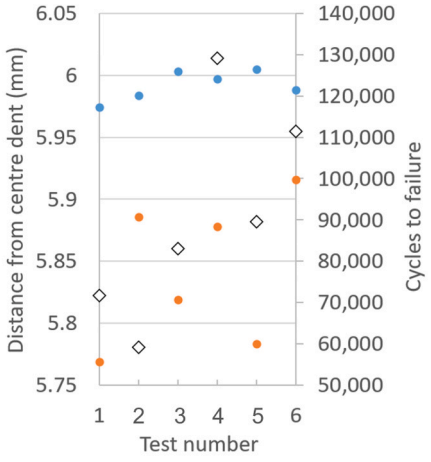

(b) Measured minimum (orange) and maximum (blue) distances between the central dent and the crack for the six tests performed. The life of each test is shown by the white diamond markers

Fig. 11. Crack position measurement features and data.

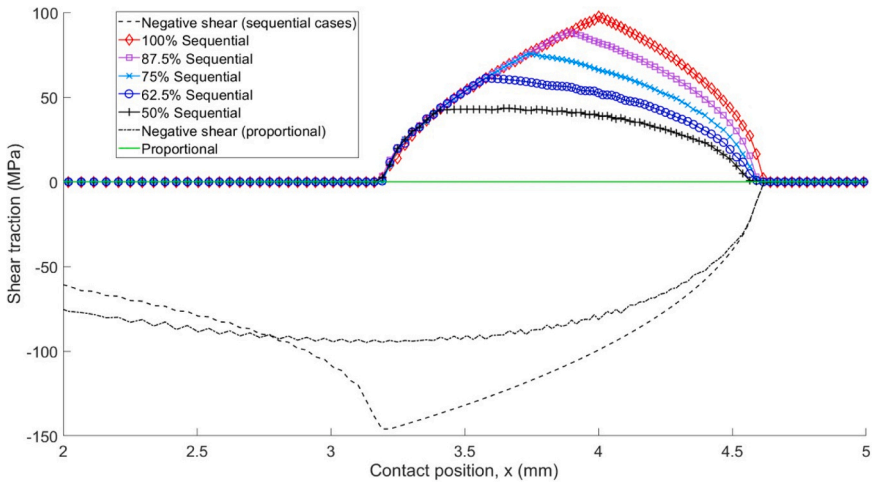

Fig. 12. Finite element output showing the changes to the shear traction distribution due to the changes in load path given in Fig. 7a. These plots show the maximum and minimum value of shear traction occurring at each point in the contact over the course of one full cycle.

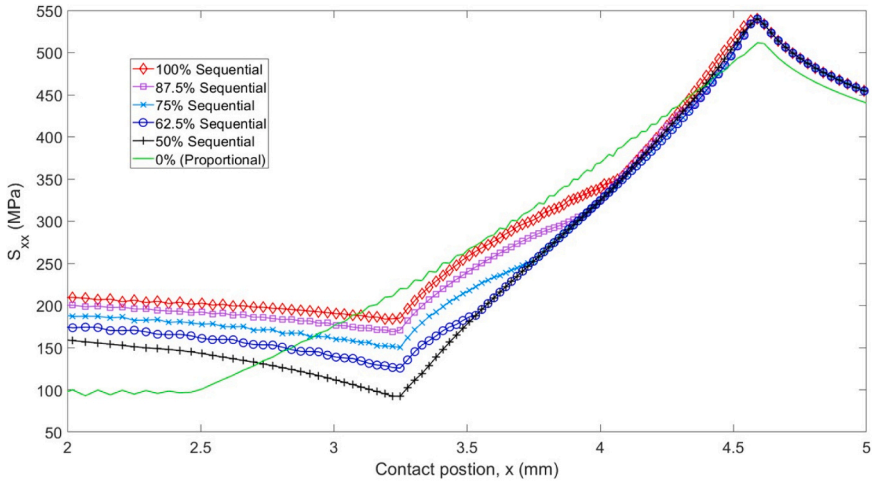

Fig. 13. Finite element output showing the changes to the Sxx stress distribution due to the changes in load path given in Fig. 6a. These plots show the range of Sxx stress over the course of one cycle.

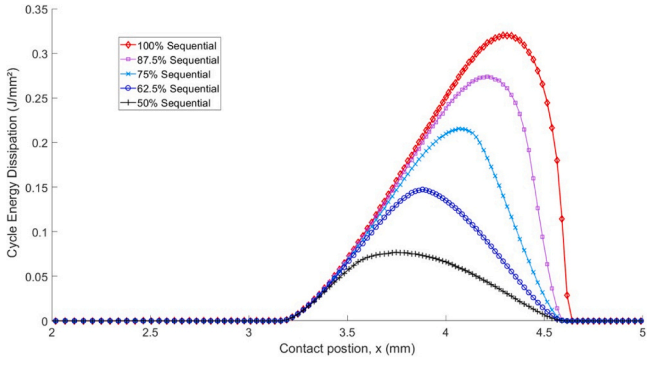

Fig. 14. Finite element output showing the changes to the dissipated energy distribution due to the changes in load path given in Fig. 6a. These plots show the energy dissipated throughout one cycle.

compared with the output from the FE models to determine where the cracks tended to initiate with respect to the peaks in pressure, dissipated energy, and range of stress parallel with the specimen surface. Fig. 15 shows plots of these data. All 6 of the tests described above were performed with the 100 % sequential load path. The graphs show the Sxx (tension parallel with the contact surface) and dissipated energy for sequential path used in the tests. Also plotted is the product of the max Sxx and the dissipated energy, better known as the Ruiz fretting fatigue damage parameter [11].

Fig. 15 shows that the average outer limit of the crack position is correlated very well with the maximum range of Sxx stress component. Note that this is not at the extreme edge of the contact at maximum size, but around 0.2 mm in from the very edge. Considering the data in Fig. 11b, the outer crack positions also have a small spread of only 31 μm. The crack positions are also shown relative to the peak dissipated energy and here, it is the average inner limit of the crack position that is correlated with the peak value. However there is a small offset of around 100 μm from the true peak. This may indicate that the dissipated energy is not as strongly correlated with damage, or that only a threshold level of dissipated energy is required for crack nucleation rather than a maximum value being preferable for crack nucleation. Previous studies in varying load path have shown changes in position of maximum dissipated energy [12]. The crack position measurements given here indicate that cracks occur at maximum Sxx range, not maximum energy. The peak of the Ruiz parameter lies on the inner crack limit.

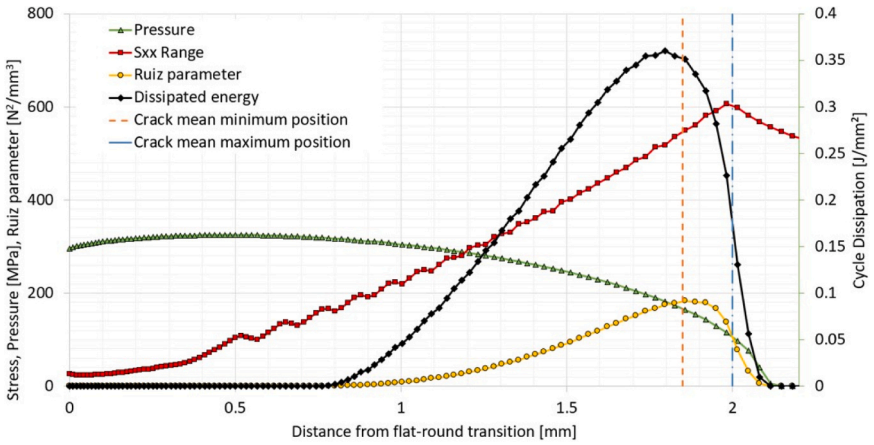

Fig. 15. Graph showing the contact pressure and the range of the stress component parallel with the contact surface (Sxx). These were obtained via FE modelling of the contact and the uneven Sxx curve is due to numerical noise from time-stepping in the model. Superimposed on this graph are vertical lines indicating the average minimum (orange) and maximum (blue) crack position corresponding to the data in Fig. 11b.

6. Conclusions

Two novel fretting fatigue experiments were presented; a load path variation allowing prevention or encouragement of slip, and a crack position measurement method giving precise and repeatable measurements. Experiments using these techniques were performed and the data were presented.

The measurement of the position of cracks relative to the contact defining body in fretting fatigue experiments is difficult due to the general lack of a well defined datum from which to measure. The introduction of a suitably small feature was shown to allow repeatable measurement of crack position, and by FE, it was shown that the presence of this feature in a well designed contact does not affect the nucleation conditions.

Through the use of this crack measurement technique, the positions of the cracks in 6 identical fretting fatigue tests were measured. The outer extreme of the 6 cracks measured had a range of just 31 μm, and the maximum value of Sxx range was within this range. A correlation between crack position and dissipated energy peak was not clear.

Eight fretting fatigue tests were performed with the same maximum and minimum values of the two load components applied (bulk and normal loads). By varying the route taken between these load points, significant changes to fretting fatigue life resulted. Tests following paths prohibiting slip produced run-outs, whilst those allowing slip resulted in short fretting fatigue lives. These differences in life were attributed to changes in shear traction and dissipated energy between tests, however with the load paths used here, decoupling these effects was not possible. This strongly encourages the design of load path variation (or other) experiments which might further decouple the effects of slip from those of stress in fretting fatigue contacts.

Declaration of Competing Interest

The authors declare that they have no known competing financial interests or personal relationships that could have appeared to influence the work reported in this paper.

Acknowledgements

James Truelove acknowledges with thanks the award of an iCASE award ref 17000027 from Rolls-Royce plc which has enabled him to carry out this work. David Hills and Luke Blades acknowledge Rolls-Royce plc and the EPSRC for their support under the Prosperity Partnership Grant “Cornerstone: Mechanical Engineering Science to Enable Aero Propulsion Futures”, Grant Ref: EP/R004951/1.

References

[1] Li X, Yang J, Li M, Zuo Z. An investigation on fretting fatigue mechanism under complex cyclic loading conditions. Int J Fatigue 2016;88:227–35.
[2] Bhatti NA, Wahab MA. Fretting fatigue crack nucleation: a review. Tribol Int 2018;121:121–38.
[3] Nesladek M, Spaniel M, Jurenka J, Růžička J, Kuželka J. Fretting fatigue–experimental and numerical approaches. Int J Fatigue 2012;44:61–73.
[4] Vingsbo O, Söderberg S. On fretting maps. Wear 1988;126(2):131–47.
[5] Sabelkin V, Mall S. Investigation into relative slip during fretting fatigue under partial slip contact condition. Fatigue Fract Eng Mater Struct 2005;28(9):809–24.
[6] Nakazawa K, Sumita M, Maruyama N. Effect of relative slip amplitude on fretting fatigue of high strength steel. Fatigue Fract Eng Mater Struct 1994;17(7):751–9.
[7] Ramesh R, Barber J, Hills D. Plane incomplete contact problems subject to bulk stress with a varying normal load. Int J Mech Sci 2017;122:228–34.
[8] Hills DA, Andresen HN. Mechanics of Fretting and Fretting Fatigue. Springer; 2021.
[9] Truelove J, Blades L, Hills D, Paynter R. Frictional half plane contacts subject tovarying normal load and bulk tension under various load paths with application to frettingfatigue experiments. Tribol Int 2023;185:108563.
[10] H. Andresen, D. Hills, A. Wormsen, and K. Macdonald, Fretting fatigue design of subsea connectors: a generalised approach to testing, In: Proceedings of the International Conference on Offshore Mechanics and Arctic Engineering, vol. 84324, p. V02AT02A036, American Society of Mechanical Engineers, 2020.
[11] Ruiz C, Boddington P, Chen K. An investigation of fatigue and fretting in a dovetail joint. Exp Mech 1984;24:208–17.
[12] Hojjati-Talemi R, Wahab MA, De Baets P. Finite element simulation of phase difference effects on fretting fatigue crack nucleation behaviour. Proc Inst Mech Eng, Part J: J Eng Tribol 2014;228(4):470–9.